

Automatic Leptonic Tensor Generation for Beyond the Standard Model (BSM) Theories

Diego Lopez Gutierrez^a Joshua Isaacson^b

^a*Macalester College,
1600 Grand Avenue, Saint Paul, MN, USA*

^b*Theory Department, Fermi National Accelerator Laboratory,
Kirk Road and Pine Street, Batavia, IL 60510*

E-mail: dlopezgu@macalester.edu, isaacson@fnal.gov

ABSTRACT: With the development of the Deep Underground Neutrino Experiment (DUNE) and Tokai-to-Hyper-Kamiokande (T2HK), we are entering the era of high-precision neutrino measurements. The colossal output of data from DUNE, plus the current data from several other neutrino experiments, will require a fast and efficient method of testing our BSM models in event generators. However, current methods for implementing a BSM theory in the event generators are prone to errors and time consuming. We propose a novel program capable of automatically calculating the leptonic tensor for a given BSM Lagrangian. This program utilizes the Universal FeynRules Output (UFO) format, the Lark package and the Berends-Giele recursive relations to produce leptonic tensors that can be automatically implemented in several neutrino event generators, including those of DUNE. We compare the results of our algorithm with analytic calculations for $e^+e^- \rightarrow \mu^+\mu^-$, $e^-\mu^- \rightarrow e^-\mu^-$ and $e^+e^- \rightarrow e^+e^-$, obtaining percentage deviations of order 10^{-14} .

Contents

1	Introduction	1
1.1	Decay Width and Cross Section	2
1.2	Lagrangian and Feynman Diagrams	2
1.3	Hadronic and Leptonic Tensor	3
2	Methods	6
2.1	Universal FeynRules Output	6
2.2	Lark Package	7
2.3	Berends-Giele Recursive Relations	8
3	Results and Discussion	10
4	Conclusion and Future Steps	11

1 Introduction

The Standard Model (SM) is our most accurate physics theory capable of describing three of the four known fundamental forces of nature along with their corresponding particles. However, the SM is an incomplete theory as it fails to explain gravity and a variety of other phenomena. For example, the SM predicts that only left-handed massless neutrinos exist, contradicting experimental evidence of massive neutrinos via neutrino oscillations as reported by the Super-Kamiokande [16], SNO [8] and KamLAND [15] experiments. Since then, several experiments have found anomalies regarding the behavior of neutrino oscillations at short-baselines, hinting at the existence of a fourth type of neutrino that is sterile to any SM interactions [4–7, 14, 17, 22]. To explain the phenomena of neutrino oscillations, the origin of its mass, the existence of a possible sterile neutrino and other interesting experimental evidence, scientists develop Beyond the Standard Model (BSM) theories. However, many BSM processes are too complex to be evaluated by hand. Instead, we rely on event generators such as Genie [9], NuWro [19], NEUT [20], and GiBUU [11, 23] to obtain predictions that we can then compare to experimental data.

Within the next decade, we are entering an era of neutrino high-precision studies. The neutrino community will be enriched with colossal amounts of data coming from the Deep Underground Neutrino Experiment (DUNE) [3] and the Tokai-to-Hyper-Kamiokande (T2HK) [1] collaborations. The unprecedented number of neutrino events coming from these two experiments, plus the data that we already have from experiments such as MicroBooNE [2], will allow for the testing of several BSM theories. However, the current method of manually implementing a BSM theory into an event generator is inadequate. The manual implementation process is prone to errors due to the different code conventions

of each event generator which inevitably lead to human errors, and is time-consuming given that the user has to repeat all the work for each BSM model. Due to these setbacks and because of the large number of theories to be tested, this current process becomes infeasible. Instead, we propose an algorithm that automatically calculates the leptonic tensor of any BSM theory given the Lagrangian. Separating the squared amplitude into its leptonic and hadronic tensor components allows us to focus on the effects of the BSM theory on the leptonic tensor. We do not focus on calculating the hadronic tensor because event generators can accomplish that within their program, and we expect any BSM effects to be mainly in the leptonic tensor, not on the hadronic tensor. Moreover, our algorithm can be easily interfaced to several neutrino event generators. The program relies on the `Universal FeynRules Output` (UFO) file [13] as well as the `Lark` package [24] and the Berends-Giele algorithm [10]. Before we dive into the details of the program, let us review the process of splitting an amplitude into its leptonic and hadronic tensors.

1.1 Decay Width and Cross Section

Among the most common observables measured in particle physics experiments are those related to the decay width (Γ) of a particle and the cross section (σ) of a process. The decay width indicates the probability per unit time that a particle of a specific kind decays. Meanwhile, the cross section tells us about the effective (cross section) area of a particle B when a particle A hits it. Both quantities give us a sense of how likely an event (whether a decay or a scattering) is to occur. We can calculate these observables following Fermi's Golden Rule for the decay width:

$$\Gamma(A_1 \rightarrow B_1 B_2 \cdots B_n) = \frac{S}{2m_A} \int d\Pi_n |\mathcal{M}_{\text{tot}}|^2 \quad (1.1)$$

and the cross section:

$$\sigma(A_1 A_2 \rightarrow B_1 B_2 \cdots B_n) = \frac{S}{2\sqrt{\lambda(s, m_{A_1}^2, m_{A_2}^2)}} \int d\Pi_n |\mathcal{M}_{\text{tot}}|^2 \quad (1.2)$$

where $|\mathcal{M}_{\text{tot}}|^2$ is the square of the total amplitude, $\lambda(s, m_{A_1}^2, m_{A_2}^2) = s^2 + m_{A_1}^4 + m_{A_2}^4 - 2(sm_{A_1}^2 + m_{A_1}^2 m_{A_2}^2 + sm_{A_2}^2)$ is the Källén function, S is a symmetry factor and $d\Pi_n$ is the n -dimensional phase space given by:

$$\int d\Pi_n = \int (2\pi)^4 \delta^{(4)} \left(\sum_i p_{A_i} - \sum_{i=1}^n p_{B_i} \right) \prod_{j=1}^n \frac{1}{2E_j} \frac{d^3 \vec{p}_j}{(2\pi)^3} \quad (1.3)$$

As we can see from Eqs. 1.1 and 1.2, the decay width Γ and the cross section σ are proportional to the squared amplitude $|\mathcal{M}_{\text{tot}}|^2$. Therefore, calculating this amplitude is necessary for obtaining the aforementioned observables.

1.2 Lagrangian and Feynman Diagrams

The Lagrangian \mathcal{L} contains all the information about the particles and interactions of a theory. It is closely related to the action (\mathcal{S}) and the least action principle ($\delta\mathcal{S} = \int d^4x \delta\mathcal{L}$) of

field theory. Quantum Electrodynamics (QED) is the quantum field theory that governs the electromagnetic interactions via the exchange of the photon γ gauge boson. Its Lagrangian is given by:

$$\mathcal{L}_{\text{QED}} = -\frac{1}{4}F_{\mu\nu}F^{\mu\nu} + \sum_{\text{all fermions}} \bar{\psi}_f i\gamma^\mu \partial_\mu \psi_f - m_f \bar{\psi}_f \psi_f + A_\mu j_f^\mu \quad (1.4)$$

where $\psi_f(\bar{\psi}_f)$ is the fermion (antifermion) field operator, A_μ is the photon field operator, $F_{\mu\nu} = \partial_\mu A_\nu - \partial_\nu A_\mu$ is the electromagnetic field strength tensor, $j_f^\mu = -eQ_f \bar{\psi}_f \gamma^\mu \psi_f$ is the electromagnetic current, and γ^μ are the gamma matrices that satisfy the anticommutation relations $\{\gamma^\mu, \gamma^\nu\} = \gamma^\mu \gamma^\nu + \gamma^\nu \gamma^\mu = 2g^{\mu\nu} \mathbb{I}_4$. For the electromagnetic processes that we are dealing with, we need to identify the term that represents the interaction of two fermions (e.g. e^-e^+) and the photon (γ). In Eq. 1.4, the term for a given fermion f corresponds to:

$$-eQ_f A_\mu \bar{\psi}_f \gamma^\mu \psi_f \quad (1.5)$$

since we have the photon and the two fermion field operators. The corresponding interaction vertex of the photon with these two fermions would then be $-ieQ_f \gamma^\mu$. This is one of the so-called Feynman rules of QED.

A Feynman diagram is a pictorial representation of a term in the perturbative expansion of the amplitude \mathcal{M}_{tot} in powers of $\alpha_{\text{EM}} = \frac{e^2}{4\pi}$, the electromagnetic coupling constant.

$$\mathcal{M}_{\text{tot}} = \sum_{\text{First-order}} \alpha^0 \mathcal{M}_0 + \sum_{\text{Second-order}} \alpha^1 \mathcal{M}_1 + \dots \quad (1.6)$$

Note that \mathcal{M}_0 contains the minimum number of α 's required for the process to occur, and this could not necessarily be proportional to α^0 . For this work, we restrict ourselves to tree-level (i.e. first-order) diagrams; that is, those diagrams with the lowest order in α . An example of a Feynman diagram is given in Fig. 1 for the $e^+e^- \rightarrow \mu^+\mu^-$ process via the exchange of a photon. A process can have more than one Feynman diagram at tree-level, in which case the Feynman diagram amplitudes are added before squaring (i.e. $|\mathcal{M}_{\text{tot}}|^2 = |\sum_i \mathcal{M}_i|^2$.) The Feynman rules to calculate amplitudes are obtained from the Lagrangian; one example would be the rule for the interaction of two fermions with a photon given above. From now on, we drop the subscript tot in the amplitude.

1.3 Hadronic and Leptonic Tensor

For neutrino interactions, neglecting double boson exchange (which is reasonable considering the uncertainties associated with the nuclear effects), we can always express the squared amplitude as:

$$|\mathcal{M}|^2 = L_{\mu\nu} H^{\mu\nu} \quad (1.7)$$

where $L_{\mu\nu}$ is the leptonic tensor and $H^{\mu\nu}$ is the hadronic tensor. To illustrate how $|\mathcal{M}|^2$ can be split into these tensors, we perform the calculation for $e^-N \rightarrow e^-N$, where N is an atomic nucleus.

First, let us consider the simpler process $e^-\mu^- \rightarrow e^-\mu^-$ with Feynman diagram given in Fig. 2. Here, we can see that the diagram is composed of an upper e^- part and a lower

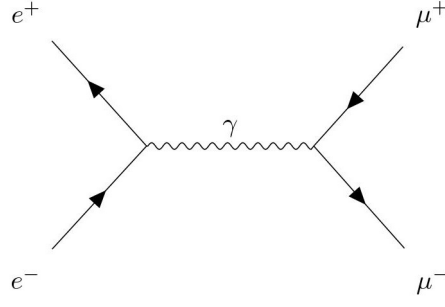


Figure 1. Feynman diagram for s-channel process $e^+e^- \rightarrow \mu^+\mu^-$.

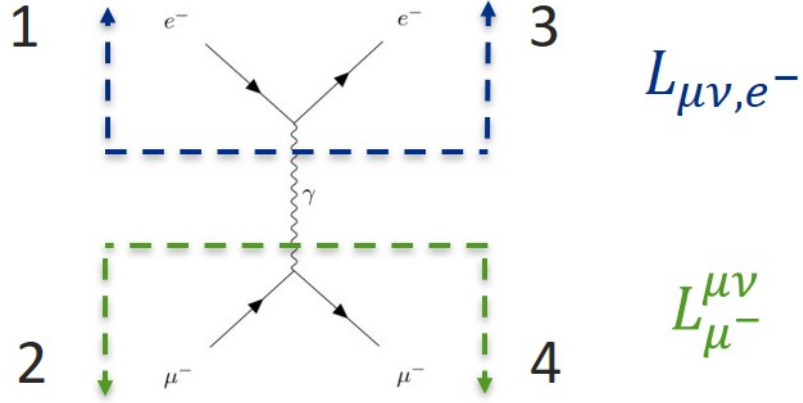


Figure 2. Feynman diagram for t-channel process $e^-\mu^- \rightarrow e^-\mu^-$. Diagram is decomposed into the electron leptonic tensor $L_{\mu\nu,e^-}$ and the muon leptonic tensor $L_{\mu^-}^{\mu\nu}$. Labeling corresponds to $e_{\text{in}}^- : 1, \mu_{\text{in}}^- : 2, e_{\text{out}}^- : 3, \mu_{\text{out}}^- : 4$.

μ^- part. This decomposition corresponds to the electron leptonic tensor, $L_{\mu\nu,e^-}$, and the muon leptonic tensor, $L_{\mu^-}^{\mu\nu}$, respectively. The process $e^-\mu^- \rightarrow e^-\mu^-$ only has one Feynman diagram at tree-level, so the total amplitude is just the amplitude corresponding to this Feynman diagram. For the calculation of the amplitude, let us first label each external particle as follows: $e_{\text{in}}^- : 1, \mu_{\text{in}}^- : 2, e_{\text{out}}^- : 3, \mu_{\text{out}}^- : 4$.

The amplitude (for given four-momenta and spin) is given by:

$$\mathcal{M} = \langle e^-(p_3, s_3) | j^\mu(0) | e^-(p_1, s_1) \rangle \frac{i g_{\mu\nu}}{(p_1 - p_3)^2} \langle \mu^-(p_4, s_4) | j^\nu(0) | \mu^-(p_2, s_2) \rangle \quad (1.8)$$

where $j^\mu(0)$ is the electromagnetic current as given in Eq. 1.4, $g_{\mu\nu}$ is the metric tensor, and p_i, s_i are the particle's four-momentum and spin respectively. Replacing the current into Eq. 1.8 and using the canonical rules, we get the following:

$$\mathcal{M} = \frac{ie^2}{(p_1 - p_3)^2} [\bar{u}_{e^-}(p_3, s_3) \gamma^\mu u_{e^-}(p_1, s_1)] [\bar{u}_{\mu^-}(p_4, s_4) \gamma_\mu u_{\mu^-}(p_2, s_2)] \quad (1.9)$$

The complex conjugate of the amplitude would be given by:

$$\mathcal{M}^* = \frac{-ie^2}{(p_1 - p_3)^2} [\bar{u}_{e^-}(\vec{p}_1, s_1) \gamma^\mu u_{e^-}(\vec{p}_3, s_3)] [\bar{u}_{\mu^-}(\vec{p}_2, s_2) \gamma_\mu u_{\mu^-}(\vec{p}_4, s_4)] \quad (1.10)$$

The square amplitude (for given momenta and spin) would be the product $\mathcal{M}\mathcal{M}^*$. However, we need to average over the initial-state spins ($\frac{1}{4} \sum_{s_1, s_2}$) and sum over all possible final-state spins (\sum_{s_3, s_4}). We then have:

$$|\mathcal{M}|^2 = \frac{e^4}{(p_1 - p_3)^4} \frac{1}{4} \sum_{s_1, s_2, s_3, s_4} [\bar{u}_{e^-}(\vec{p}_3, s_3) \gamma^\mu u_{e^-}(\vec{p}_1, s_1)] [\bar{u}_{e^-}(\vec{p}_1, s_1) \gamma^\mu u_{e^-}(\vec{p}_3, s_3)] \times \quad (1.11)$$

$$[\bar{u}_{\mu^-}(\vec{p}_4, s_4) \gamma_\mu u_{\mu^-}(\vec{p}_2, s_2)] [\bar{u}_{\mu^-}(\vec{p}_2, s_2) \gamma_\mu u_{\mu^-}(\vec{p}_4, s_4)]$$

Using the spin-sum relations for Dirac spinors¹, the Dirac equation relations² and the trace relations³, we obtain the following result:

$$|\mathcal{M}|^2 = \frac{4e^4}{(p_1 - p_3)^4} [p_{3\mu} p_{1\nu} + p_{3\nu} p_{1\mu} + (m_e^2 - p_1 \cdot p_3) g_{\mu\nu}] [p_4^\mu p_2^\nu + p_4^\nu p_2^\mu + (m_\mu^2 - p_2 \cdot p_4) g^{\mu\nu}] \quad (1.12)$$

Notice that the first term only depends on the electron momenta and the second term only depends on the muon momenta. Let us define the tensors:

$$L_{\mu\nu, e^-} = \frac{2e^2}{(p_1 - p_3)^2} [p_{3\mu} p_{1\nu} + p_{3\nu} p_{1\mu} + (m_e^2 - p_1 \cdot p_3) g_{\mu\nu}] \quad (1.13a)$$

$$L_{\mu^-}^{\mu\nu} = \frac{2e^2}{(p_2 - p_4)^2} [p_4^\mu p_2^\nu + p_4^\nu p_2^\mu + (m_\mu^2 - p_2 \cdot p_4) g^{\mu\nu}] \quad (1.13b)$$

recalling that, by conservation of four-momentum, $(p_1 - p_3) = (p_2 - p_4)$. Our final squared amplitude is then expressed as:

$$|\mathcal{M}|^2 = L_{\mu\nu, e^-} L_{\mu^-}^{\mu\nu} \quad (1.14)$$

Let us now examine the process $e^- N \rightarrow e^- N$. The Feynman diagram for this interaction is given in Fig. 3. As we can see, the diagram is very similar to that in Fig. 2. In fact, the upper electron part is the same for both cases. When calculating the amplitude for this process, we will obtain one term that only depends on the electron momenta and one term that only depends on the nucleus momenta. Depending on the energy, the electron may scatter off of a proton, a neutron or the nucleus itself. At high enough energies, it can scatter off of the partons inside the protons and neutrons. Since the interaction of the photon with the nucleus depends on complex nuclear physics and nuclear form factors, and on the energy of the interaction, we will simply denote this second term by $H_N^{\mu\nu}$, the hadronic tensor. We will leave the complex nuclear physics to the neutrino event generators.

¹ $\sum_{s=\pm 1/2} u_f(\vec{p}, s) \bar{u}_f(\vec{p}, s) = \not{p} + m_f$

² $(\not{p} - m_f) u_f(\vec{p}, s) = \bar{u}_f(\vec{p}, s) (\not{p} - m_f) = 0$

³ $\text{Tr}[\gamma^\mu] = 0$, $\text{Tr}[\text{odd number of } \gamma^\mu] = 0$, $\text{Tr}[\gamma^\mu \gamma^\nu] = 4g^{\mu\nu}$, $\text{Tr}[\gamma^\mu \gamma^\nu \gamma^\sigma \gamma^\rho] = 4(g^{\mu\nu} g^{\sigma\rho} - g^{\mu\sigma} g^{\nu\rho} + g^{\mu\rho} g^{\nu\sigma})$

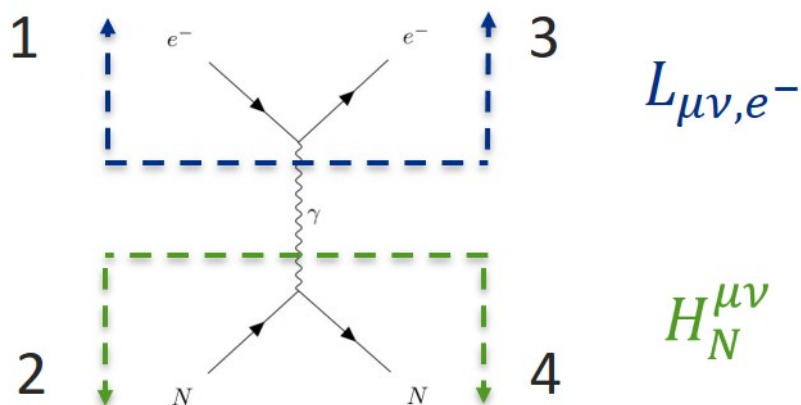


Figure 3. Feynman diagram for t-channel process $e^- N \rightarrow e^- N$. Diagram is decomposed into the electron leptonic tensor $L_{\mu\nu, e^-}$ and the nucleus hadronic tensor $H_N^{\mu\nu}$. Labeling corresponds to $e_{\text{in}}^- : 1$, $N_{\text{in}} : 2$, $e_{\text{out}}^- : 3$, $N_{\text{out}} : 4$.

Thus, similarly to Eq. 1.14, the squared amplitude for the process $e^- N \rightarrow e^- N$ is given by:

$$|\mathcal{M}|^2 = L_{\mu\nu, e^-} H_N^{\mu\nu} \quad (1.15)$$

where $L_{\mu\nu, e^-} = \frac{2g^2}{(p_1 - p_3)^2} \left[p_{3\mu} p_{1\nu} + p_{3\nu} p_{1\mu} + (m_e^2 - p_1 \cdot p_3) g_{\mu\nu} - i\varepsilon_{\mu\nu\alpha\beta} p_1^\alpha p_3^\beta \right]$. Notice that we have added a term to $L_{\mu\nu, e^-}$ that did not appear in Eq. 1.13a. For the case of the photon, the extra term cancels out in Eq. 1.14 because the photon couples equally to both left- and right-handed particles. However, if instead of a photon, we had had a Z boson, which discriminates between left- and right-handed particles, the extra term would not have cancelled out. Here we are talking about a general interaction between the leptonic and hadronic tensors, therefore in Eq. 1.15, we have decided to include the extra term for generality.

2 Methods

Now that we reviewed how to split a squared amplitude into its leptonic and hadronic tensor components, we can dive into the details of our program.

2.1 Universal FeynRules Output

Given a BSM Lagrangian, we utilize the `FeynRules` Mathematica package to calculate the vertices of a theory and store its information [12]. This output from `FeynRules` can be interfaced and exported as a `Universal FeynRules Output (UFO)` [13] file, which contains all the necessary information of the theory encoded into Python modules. More importantly, the `UFO` format is designed to be agnostic. That is, the program does not make any prior assumptions on the different Lorentz and color structures allowed in the theory as well as on the number of particles. Because of this lack of assumptions, the `UFO` file also allows for a larger compatibility with event generators, thus making it ‘universal’.

As part of this compatibility, the UFO file stores the information of the theory as instances of Python classes. In particular, all the instances of particles, parameters, Lorentz and color structures, couplings and vertices are stored in their own Python module, ready to be interfaced with computer codes. However, these objects are stored as strings that represent mathematical objects. For example, the electromagnetic vertex for e^+e^- annihilation

$$ie\gamma^\mu \tag{2.1}$$

would be stored as:

```
V_77 = Vertex(name = 'V_77',
              particles = [ P.e__plus__, P.e__minus__, P.a ],
              color = [ '1' ],
              lorentz = [ L.FFV1 ],
              couplings = {(0,0):C.GC_3})
```

with Lorentz structure

```
FFV1 = Lorentz(name = 'FFV1',
               spins = [ 2, 2, 3 ],
               structure = 'Gamma(3,2,1)')
```

and coupling

```
GC_3 = Coupling(name = 'GC_3',
                 value = '-(ee*complex(0,1))',
                 order = {'QED':1})
```

As we can see in the attributes `color` for the vertex class, `structure` for the Lorentz class and `value` for the coupling class, the instances are strings symbolizing mathematical expressions. In particular, we have:

$$'1' = \mathbb{I}, \quad \text{'Gamma(3,2,1)'} = (\gamma^{\mu_3})_{i_2, i_1}, \quad \text{'-(ee*complex(0,1))'} = -ie.$$

To transform these Python strings into useful mathematical objects with which we can perform calculations, we utilize the `Lark` package.

2.2 Lark Package

The `Lark` package is a parser in Python compatible with most programming and natural languages [24]. For this project, we developed a `Lark` grammar for the UFO output strings, and a Python module containing the classes that would mathematically represent these strings. For the case of `'Gamma(3,2,1)'`, we have for example:

```
'Gamma(3,2,1)':
Tensor([[[ 0.+0.j  0.+0.j  1.+0.j  0.+0.j]
         [ 0.+0.j  0.+0.j  0.+0.j  1.+0.j]
         [ 1.+0.j  0.+0.j  0.+0.j  0.+0.j]
         [ 0.+0.j  1.+0.j  0.+0.j  0.+0.j]])
```

```

[[ [ 0.+0.j 0.+0.j 0.+0.j 1.+0.j ]
  [ 0.+0.j 0.+0.j 1.+0.j 0.+0.j ]
  [ 0.+0.j -1.+0.j 0.+0.j 0.+0.j ]
  [-1.+0.j 0.+0.j 0.+0.j 0.+0.j ]]]

[[ [ 0.+0.j 0.+0.j 0.+0.j -0.-1.j ]
  [ 0.+0.j 0.+0.j 0.+1.j 0.+0.j ]
  [ 0.+0.j 0.+1.j 0.+0.j 0.+0.j ]
  [-0.-1.j 0.+0.j 0.+0.j 0.+0.j ]]]

[[ [ 0.+0.j 0.+0.j 1.+0.j 0.+0.j ]
  [ 0.+0.j 0.+0.j 0.+0.j -1.+0.j ]
  [-1.+0.j 0.+0.j 0.+0.j 0.+0.j ]
  [ 0.+0.j 1.+0.j 0.+0.j 0.+0.j ]]],
(Index(3, True), Index(2, False), Index(1, False))

```

which is a Tensor object with Lorentz (True) and spin (False) indices that we have defined. Here we use the Weyl Representation of the γ matrices. Our grammar is able to deal with all the Lorentz and color structures, as well as with parameters and couplings. Now that we have all the information available in mathematical objects, we proceed to calculate the squared amplitudes.

2.3 Berends-Giele Recursive Relations

For the calculation of the amplitudes, we utilize the Berends-Giele recursive relations [10]. This algorithm recursively breaks down each Feynman diagram into currents J_i^α that act as building blocks. Because of its nature, the Berends-Giele recursive relations allow us to recycle diagrams' components in different calculations, thus significantly increasing the efficiency of the program and its speed. The program brings down the computational scaling from $\mathcal{O}(n!)$ to $\mathcal{O}(e^n)$. The Berends-Giele relations were initially proposed for color-ordered multi-parton amplitudes for n -gluons [10]. Since then, the algorithm has been extended to deal with 3-point vertices (not just gluons) implemented in the matrix-element generator Comix [18] and further generalized to deal with n -point vertices at tree-level [21]. In this work, we implemented only 3- and 4-point vertices. For all renormalizable field theories, these are all the allowed vertices.

The Berends-Giele current for a 3-point vertex is given by the following expression:

$$J_i^\alpha(\pi) = P_i(\pi) \sum_{V_i^{j,k}} \sum_{\{\pi_1, \pi_2\} \in P_2(\pi)} S(\pi_1, \pi_2) V_i^{j,k}(\pi_1, \pi_2) J_j^\beta(\pi_1) J_k^\rho(\pi_2) \quad (2.2)$$

where π is a set of N particles, π_1, π_2 are set partitions of π , $P_i(\pi)$ is a propagator term, $J_j^\beta(\pi_1)$ and $J_k^\rho(\pi_2)$ are the currents adjacent to J_i^α and for given partitions π_1, π_2 , $V_i^{j,k}$ is the vertex connecting these three currents, and $S(\pi_1, \pi_2)$ is a symmetry factor for the corresponding set partition of π [18]. The sum is over all set partitions of π into π_1, π_2 and for all the existing 3-point vertices of the currents. The current of a single external particle is its wavefunction. A pictorial representation of this current can be found in Fig. 4 for a photon-muon vertex.

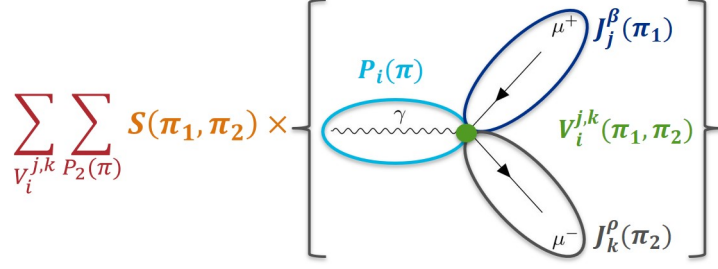


Figure 4. Pictorial color-coded representation of the Berends-Giele recursive relations' current J_i^α . This case represents the current for a photon-muon vertex. In this case, $\pi = \{\mu^-, \mu^+\}$ and $\pi_1 = \{\mu^+\}, \pi_2 = \{\mu^-\}$.

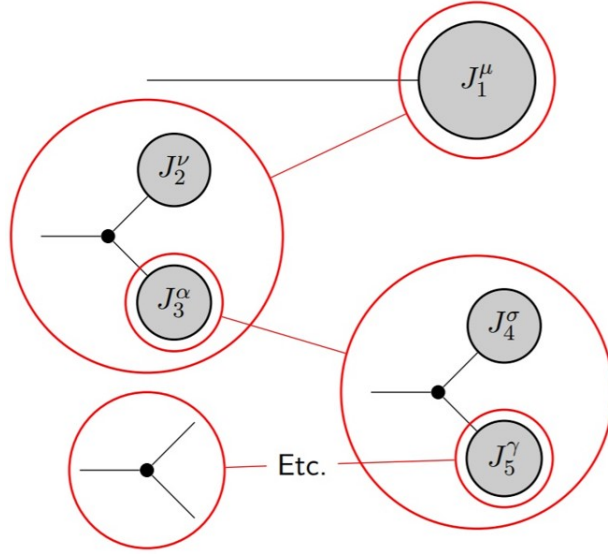


Figure 5. Schematic of the recursive calculation of an amplitude $\mathcal{M}(\pi)$ following the Berends-Giele process. The amplitude is recursively broken down into current J_1^μ and consequent sub-currents J_2^ν, J_3^α , etc.

With the expression for the current given in Eq. 2.2, we calculate the amplitude for a set π of N particles as follows:

$$\mathcal{M}(\pi) = J_n^\alpha(\pi) \cdot \frac{1}{P_{\bar{n}}(\pi \setminus n)} \cdot J_{\bar{n}}^\alpha(\pi \setminus n) \quad (2.3)$$

where $\mathcal{M}(\pi)$ is the amplitude for the set π , $J_n^\alpha(\pi)$ is the corresponding current for particle n , \bar{n} denotes reversed particle properties (e.g. opposite momentum, particle type, helicity, etc.), $P_{\bar{n}}(\pi \setminus n)$ is the propagator term for the set of particles $\pi \setminus n$ and $J_{\bar{n}}^\alpha(\pi \setminus n)$ is the current following the convention of \bar{n} for the set $\pi \setminus n$. The algorithm breaks each Feynman diagram into currents with corresponding sub-currents. The end point of the recursion is when the algorithm finds an external particle, at which point the current is decomposed into the particle's wavefunction. A schematic of the recursive process for the amplitude calculation is given in Fig. 5, and an example for $e^+e^- \rightarrow \mu^+\mu^-$ can be found in Fig. 6

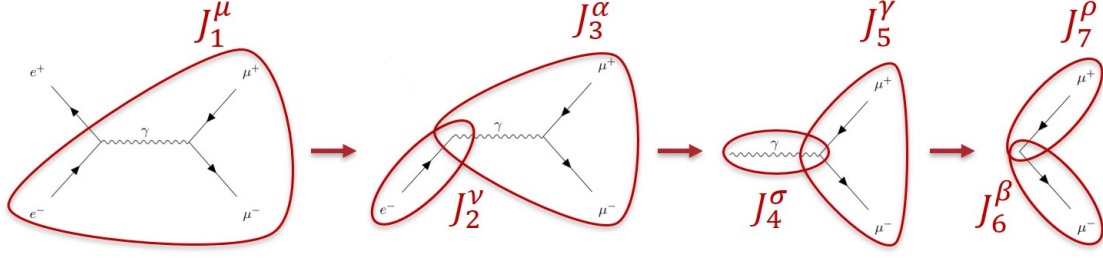


Figure 6. Example of recursive calculation of an amplitude $\mathcal{M}(\pi)$ for the process $e^+e^- \rightarrow \mu^+\mu^-$. The algorithm breaks down each Feynman diagram until it reaches external particle currents.

As can be deduced from Figs. 5 and 6, one important advantage of this method is that we can reuse the currents for other Feynman diagram calculations within a given process.

3 Results and Discussion

To test our program, we calculated the squared amplitudes $|\mathcal{M}|^2$ for three different Standard Model ($e^+e^- \rightarrow \mu^+\mu^-$, $e^-\mu^- \rightarrow e^-\mu^-$, $e^+e^- \rightarrow e^+e^-$) processes. These calculations serve as validation results to show that we can expand our program to compute more complex processes or test BSM theories.

The analytic squared amplitudes of these SM processes are given in terms of the Mandelstam variables. Let us label each 2-to-2 process by $12 \rightarrow 34$. Then we define:

$$s = (p_1 + p_2)^2 = (p_3 + p_4)^2 \quad (3.1a)$$

$$t = (p_1 - p_3)^2 = (p_2 - p_4)^2 \quad (3.1b)$$

$$u = (p_1 - p_4)^2 = (p_2 - p_3)^2 \quad (3.1c)$$

For illustrative purposes, let us calculate the analytic solution for $e^-\mu^- \rightarrow e^-\mu^-$. Recall Eq. 1.12. First, notice that $(p_1 - p_3)^4 = t^2$. For our calculations, we are dealing with high enough energies (i.e. $E \gg m_e, m_\mu$) so that we can neglect the particles' masses. Our amplitude in Eq. 1.12 is then:

$$|\mathcal{M}|^2 = \frac{4e^4}{t^2} [p_{3\mu}p_{1\nu} + p_{3\nu}p_{1\mu} - p_1 \cdot p_3 g_{\mu\nu}] [p_4^\mu p_2^\nu + p_4^\nu p_2^\mu - p_2 \cdot p_4 g^{\mu\nu}]$$

$$|\mathcal{M}|^2 = \frac{8e^4}{t^2} [(p_3 \cdot p_4)(p_1 \cdot p_2) + (p_3 \cdot p_2)(p_1 \cdot p_4)]$$

Notice that, because we are assuming $m_e = m_\mu = 0$, we also get:

$$s = (p_1 + p_2)^2 = p_1^2 + p_2^2 + 2p_1 \cdot p_2 = m_e^2 + m_\mu^2 + 2p_1 \cdot p_2 = 2p_1 \cdot p_2 = 2p_3 \cdot p_4$$

$$u = (p_1 - p_4)^2 = p_1^2 + p_4^2 - 2p_1 \cdot p_4 = m_e^2 + m_\mu^2 - 2p_1 \cdot p_4 = -2p_1 \cdot p_4 = -2p_2 \cdot p_3$$

and:

$$s^2 = 4(p_1 \cdot p_2)(p_3 \cdot p_4)$$

$$u^2 = 4(p_1 \cdot p_4)(p_2 \cdot p_3)$$

Then the initial-state spin-averaged and final-state spin-summed amplitude is:

$$|\mathcal{M}|^2 = 2e^4 \frac{s^2 + u^2}{t^2} \quad (3.4)$$

The analytic solutions for spin-summed (without the $\frac{1}{4}$ factor) squared amplitudes would then be:

$$|\mathcal{M}(e^+e^- \rightarrow \mu^+\mu^-)|^2 = 8e^4 \left(\frac{t^2 + u^2}{s^2} \right) \quad (3.5a)$$

$$|\mathcal{M}(e^-\mu^- \rightarrow e^-\mu^-)|^2 = 8e^4 \left(\frac{s^2 + u^2}{t^2} \right) \quad (3.5b)$$

$$|\mathcal{M}(e^+e^- \rightarrow e^+e^-)|^2 = 8e^4 \left(\frac{u^2 + s^2}{t^2} + 2\frac{u^2}{st} + \frac{u^2 + t^2}{s^2} \right) \quad (3.5c)$$

We calculate these amplitudes in our algorithm.

The results for $e^+e^- \rightarrow \mu^+\mu^-$ can be found in Fig. 7, for $e^-\mu^- \rightarrow e^-\mu^-$ can be found in Fig. 8 and for $e^+e^- \rightarrow e^+e^-$ can be found in Fig. 9. For these processes, we computed the analytic and computational squared amplitudes for 500 equally-spaced values of $\cos(\theta)$, the cosine of the polar angle θ , in the range $[-1, 1)$. Throughout the calculations, the value of the azimuthal angle ϕ was randomly selected to be $\phi = 0.34$ for $e^+e^- \rightarrow \mu^+\mu^-$, $\phi = 2.67$ for $e^-\mu^- \rightarrow e^-\mu^-$, and $\phi = 0.00$ for $e^+e^- \rightarrow e^+e^-$. Note that the amplitudes do not depend on the choice of azimuthal angle. The left panels of Figs. 7, 8 and 9 show the computational and analytic amplitudes plotted versus $\cos(\theta)$, where the computational and analytic amplitudes overlap almost perfectly. On the right panels, we plotted the percentage deviations of the amplitude with respect to the analytic solution (i.e. $\frac{\delta|\mathcal{M}|^2}{|\mathcal{M}|_{\text{ana}}^2}$). As could be deduced from the left panels, the percentage deviations are minimal and of order 10^{-14} , with the largest deviations at the beginning and end of the $\cos(\theta)$ range. These deviations are most likely due to the numerical precision of the calculations. Therefore, in the corners of the phase space, the numerical deviations are larger. These deviations are close to the machine precision error which means our results are accurate to an acceptable precision without need to worry for the deviations.

4 Conclusion and Future Steps

In this work, we coded a program that automatically calculates the squared amplitude of Standard Model processes. For the development of our algorithm, we utilized the `Universal FeynRules Output` (UFO) [13] file format to obtain the relevant information of the theory, and relied on the Lark package [24] and the Berends-Giele recursive relations [10] for 3- and 4-point vertices for proper parsing and computation of the squared amplitudes. Validation tests for the SM processes $e^+e^- \rightarrow \mu^+\mu^-$, $e^-\mu^- \rightarrow e^-\mu^-$, and $e^+e^- \rightarrow e^+e^-$ are presented in Sec. 3 and show promising results, with percentage deviations (10^{-14}) of similar magnitude to machine precision errors. Future steps for this project involve transforming the squared amplitude into a leptonic tensor as exemplified in Sec. 1.3. These leptonic tensors will let us easily interface our program with several neutrino event

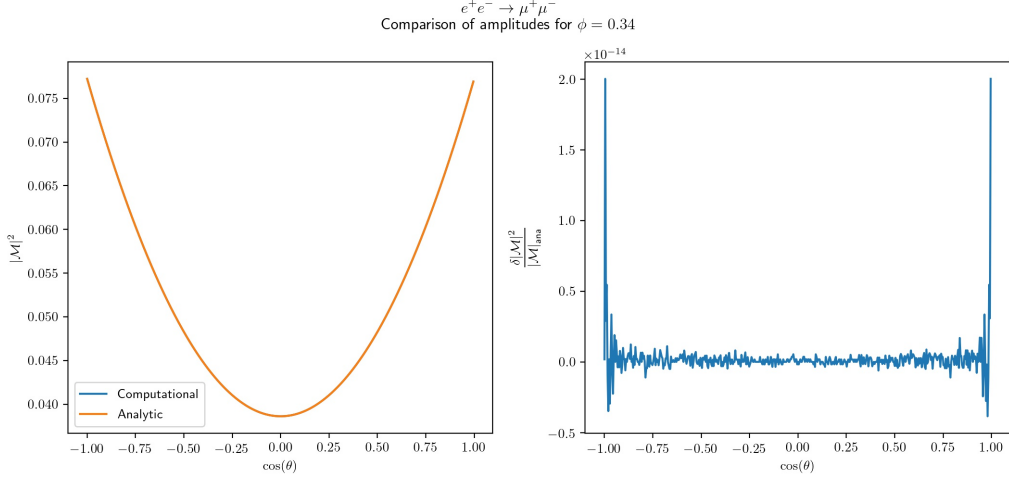


Figure 7. Validation results for the process $e^+e^- \rightarrow \mu^+\mu^-$ with random azimuthal angle $\phi = 0.34$ and for 500 evenly-spaced values of $\cos(\theta)$ in the range $[-1, 1)$. On the left panel, we plot the computational and analytic squared amplitudes versus $\cos(\theta)$. On the right panel, we plot the percentage deviation of the squared amplitude with respect to the analytic value as a function of $\cos(\theta)$.

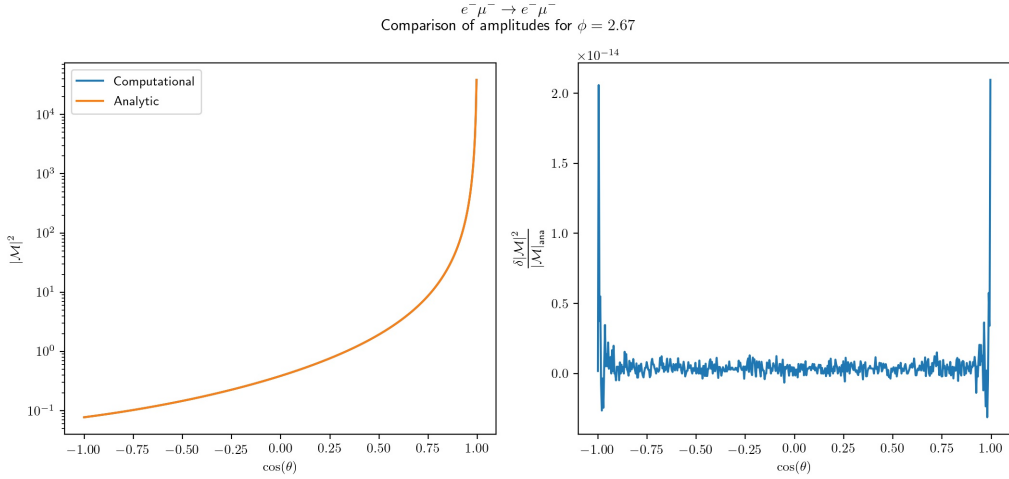


Figure 8. Validation results for the process $e^-\mu^- \rightarrow e^-\mu^-$ with random azimuthal angle $\phi = 2.67$ and for 500 evenly-spaced values of $\cos(\theta)$ in the range $[-1, 1)$. On the left panel, we plot the computational and analytic squared amplitudes versus $\cos(\theta)$. On the right panel, we plot the percentage deviation of the squared amplitude with respect to the analytic value as a function of $\cos(\theta)$.

generators. Once we can extract the leptonic tensor from the squared amplitudes, we plan on performing tests with more complex events as well as with some Beyond the Standard Model theories.

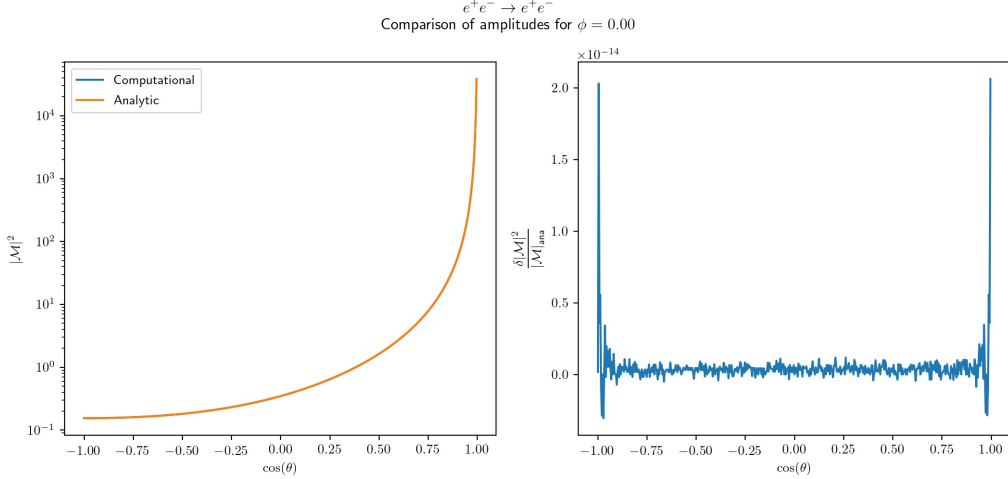


Figure 9. Validation results for the process $e^+e^- \rightarrow e^+e^-$ with random azimuthal angle $\phi = 0.00$ and for 500 evenly-spaced values of $\cos(\theta)$ in the range $[-1, 1)$. On the left panel, we plot the computational and analytic squared amplitudes versus $\cos(\theta)$. On the right panel, we plot the percentage deviation of the squared amplitude with respect to the analytic value as a function of $\cos(\theta)$.

Acknowledgments

This manuscript has been authored by Fermi Research Alliance, LLC under Contract No. DE-AC02-07CH11359 with the U.S. Department of Energy, Office of Science, Office of High Energy Physics.

FERMILAB-FN-1103-T

References

- [1] K. Abe et al. Physics potential of a long-baseline neutrino oscillation experiment using a J-PARC neutrino beam and Hyper-Kamiokande. *PTEP*, 2015:053C02, 2015.
- [2] P. Abratenko, C. Adams, M. Alrashed, R. An, J. Anthony, J. Asaadi, A. Ashkenazi, M. Auger, S. Balasubramanian, B. Baller, C. Barnes, G. Barr, M. Bass, F. Bay, A. Bhat, K. Bhattacharya, M. Bishai, A. Blake, T. Bolton, L. Camilleri, D. Caratelli, I. Caro Terrazas, R. Carr, R. Castillo Fernandez, F. Cavanna, G. Cerati, Y. Chen, E. Church, D. Cianci, E. O. Cohen, G. H. Collin, J. M. Conrad, M. Convery, L. Cooper-Troendle, J. I. Crespo-Anad3n, M. Del Tutto, D. Devitt, A. Diaz, L. Domine, K. Duffy, S. Dytman, B. Eberly, A. Ereditato, L. Escudero Sanchez, J. Esquivel, J. J. Evans, R. S. Fitzpatrick, B. T. Fleming, D. Franco, A. P. Furmanski, D. Garcia-Gamez, V. Genty, D. Goeldi, S. Gollapinni, O. Goodwin, E. Gramellini, H. Greenlee, R. Grosso, L. Gu, W. Gu, R. Guenette, P. Guzowski, A. Hackenburg, P. Hamilton, O. Hen, C. Hill, G. A. Horton-Smith, A. Hourlier, E.-C. Huang, C. James, J. Jan de Vries, X. Ji, L. Jiang, R. A. Johnson, J. Joshi, H. Jostlein, Y.-J. Jwa, G. Karagiorgi, W. Ketchum, B. Kirby, M. Kirby, T. Kobilarcik, I. Kreslo, I. Lepetic, Y. Li, A. Lister, B. R. Littlejohn, S. Lockwitz, D. Lorca, W. C. Louis, M. Luethi, B. Lundberg, X. Luo, A. Marchionni, S. Marocco, C. Mariani, J. Marshall, J. Martin-Albo, D. A. Martinez Caicedo, K. Mason, A. Mastbaum, V. Meddage, T. Mettler, J. Mills, K. Mistry,

- A. Mogan, J. Moon, M. Mooney, C. D. Moore, J. Mousseau, M. Murphy, R. Murrells, D. Naples, P. Nienaber, J. Nowak, O. Palamara, V. Pandey, V. Paolone, A. Papadopoulou, V. Papavassiliou, S. F. Pate, Z. Pavlovic, E. Piasetzky, D. Porzio, G. Pulliam, X. Qian, J. L. Raaf, A. Rafique, L. Ren, L. Rochester, H. E. Rogers, M. Ross-Lonergan, C. Rudolf von Rohr, B. Russell, G. Scanavini, D. W. Schmitz, A. Schukraft, W. Seligman, M. H. Shaevitz, R. Sharankova, J. Sinclair, A. Smith, E. L. Snider, M. Soderberg, S. Söldner-Rembold, S. R. Soleti, P. Spentzouris, J. Spitz, M. Stancari, J. St. John, T. Strauss, K. Sutton, S. Sword-Fehlberg, A. M. Szelc, N. Tagg, W. Tang, K. Terao, M. Thomson, R. T. Thornton, M. Touns, Y.-T. Tsai, S. Tufanli, T. Usher, W. Van De Pontseele, R. G. Van de Water, B. Viren, M. Weber, H. Wei, D. A. Wickremasinghe, K. Wierman, Z. Williams, S. Wolbers, T. Wongjirad, K. Woodruff, W. Wu, T. Yang, G. Yarbrough, L. E. Yates, G. P. Zeller, J. Zennamo, and C. Zhang. First Measurement of Inclusive Muon Neutrino Charged Current Differential Cross Sections on Argon at $E_\nu \sim 0.8$ GeV with the MicroBooNE Detector. Phys. Rev. Lett., 123:131801, Sep 2019.
- [3] R. Acciarri et al. Long-Baseline Neutrino Facility (LBNF) and Deep Underground Neutrino Experiment (DUNE): Conceptual Design Report, Volume 2: The Physics Program for DUNE at LBNF. 12 2015.
- [4] Mario A. Acero, Carlo Giunti, and Marco Laveder. Limits on ν_e and $\bar{\nu}_e$ disappearance from Gallium and reactor experiments. Phys. Rev. D, 78:073009, Oct 2008.
- [5] A. Aguilar, L. B. Auerbach, R. L. Burman, D. O. Caldwell, E. D. Church, A. K. Cochran, J. B. Donahue, A. Fazely, G. T. Garvey, R. M. Gunasingha, R. Imlay, W. C. Louis, R. Majkic, A. Malik, W. Metcalf, G. B. Mills, V. Sandberg, D. Smith, I. Stancu, M. Sung, R. Tayloe, G. J. VanDalen, W. Vernon, N. Wadia, D. H. White, and S. Yellin. Evidence for neutrino oscillations from the observation of $\bar{\nu}_e$ appearance in a $\bar{\nu}_\mu$ beam. Phys. Rev. D, 64:112007, Nov 2001.
- [6] A. A. Aguilar-Arevalo, C. E. Anderson, S. J. Brice, B. C. Brown, L. Bugel, J. M. Conrad, R. Dharmapalan, Z. Djurcic, B. T. Fleming, R. Ford, F. G. Garcia, G. T. Garvey, J. Mirabal, J. Grange, J. A. Green, R. Imlay, R. A. Johnson, G. Karagiorgi, T. Katori, T. Kobilarcik, S. K. Linden, W. C. Louis, K. B. M. Mahn, W. Marsh, C. Mauger, W. Metcalf, G. B. Mills, C. D. Moore, J. Mousseau, R. H. Nelson, V. Nguyen, P. Nienaber, J. A. Nowak, B. Osmanov, Z. Pavlovic, D. Perevalov, C. C. Polly, H. Ray, B. P. Roe, A. D. Russell, R. Schirato, M. H. Shaevitz, M. Sorel, J. Spitz, I. Stancu, R. J. Stefanski, R. Tayloe, M. Tzanov, R. G. Van de Water, M. O. Wascko, D. H. White, M. J. Wilking, G. P. Zeller, and E. D. Zimmerman. Event Excess in the MiniBooNE Search for $\bar{\nu}_\mu \rightarrow \bar{\nu}_e$ Oscillations. Phys. Rev. Lett., 105:181801, Oct 2010.
- [7] A. A. Aguilar-Arevalo, B. C. Brown, L. Bugel, G. Cheng, J. M. Conrad, R. L. Cooper, R. Dharmapalan, A. Diaz, Z. Djurcic, D. A. Finley, R. Ford, F. G. Garcia, G. T. Garvey, J. Grange, E.-C. Huang, W. Huelsnitz, C. Ignarra, R. A. Johnson, G. Karagiorgi, T. Katori, T. Kobilarcik, W. C. Louis, C. Mariani, W. Marsh, G. B. Mills, J. Mirabal, J. Monroe, C. D. Moore, J. Mousseau, P. Nienaber, J. Nowak, B. Osmanov, Z. Pavlovic, D. Perevalov, H. Ray, B. P. Roe, A. D. Russell, M. H. Shaevitz, J. Spitz, I. Stancu, R. Tayloe, R. T. Thornton, M. Tzanov, R. G. Van de Water, D. H. White, D. A. Wickremasinghe, and E. D. Zimmerman. Significant Excess of Electronlike Events in the MiniBooNE Short-Baseline Neutrino Experiment. Phys. Rev. Lett., 121:221801, Nov 2018.
- [8] Q.R. Ahmad et al. Direct evidence for neutrino flavor transformation from neutral current interactions in the Sudbury Neutrino Observatory. Phys. Rev. Lett., 89:011301, 2002.

- [9] C. Andreopoulos et al. The GENIE Neutrino Monte Carlo Generator. Nucl. Instrum. Meth. A, 614:87–104, 2010.
- [10] Frits A. Berends and W.T. Giele. Recursive Calculations for Processes with n Gluons. Nucl. Phys. B, 306:759–808, 1988.
- [11] O. Buss, T. Gaitanos, K. Gallmeister, H. van Hees, M. Kaskulov, O. Lalakulich, A. B. Larionov, T. Leitner, J. Weil, and U. Mosel. Transport-theoretical Description of Nuclear Reactions. Phys. Rept., 512:1–124, 2012.
- [12] Neil D. Christensen and Claude Duhr. FeynRules - Feynman rules made easy. Comput. Phys. Commun., 180:1614–1641, 2009.
- [13] Celine Degrande, Claude Duhr, Benjamin Fuks, David Grellscheid, Olivier Mattelaer, and Thomas Reiter. UFO - The Universal FeynRules Output. Comput. Phys. Commun., 183:1201–1214, 2012.
- [14] Mona Dentler, Álvaro Hernández-Cabezudo, Joachim Kopp, Michele Maltoni, and Thomas Schwetz. Sterile neutrinos or flux uncertainties? — Status of the reactor anti-neutrino anomaly. JHEP, 11:099, 2017.
- [15] K. Eguchi et al. First results from KamLAND: Evidence for reactor anti-neutrino disappearance. Phys. Rev. Lett., 90:021802, 2003.
- [16] Y. Fukuda et al. Measurement of the flux and zenith angle distribution of upward through going muons by Super-Kamiokande. Phys. Rev. Lett., 82:2644–2648, 1999.
- [17] Carlo Giunti and Marco Laveder. Statistical significance of the gallium anomaly. Phys. Rev. C, 83:065504, Jun 2011.
- [18] Tanju Gleisberg and Stefan Hoeche. Comix, a new matrix element generator. JHEP, 12:039, 2008.
- [19] Tomasz Golan, Cezary Juszczak, and Jan T. Sobczyk. Final State Interactions Effects in Neutrino-Nucleus Interactions. Phys. Rev., C86:015505, 2012.
- [20] Y. Hayato. NEUT. Nucl. Phys. B Proc. Suppl., 112:171–176, 2002.
- [21] Stefan H"ocher, Silvan Kuttimalai, Steffen Schumann, and Frank Siegert. Beyond Standard Model calculations with Sherpa. Eur. Phys. J. C, 75(3):135, 2015.
- [22] G. Mention, M. Fechner, Th. Lasserre, Th. A. Mueller, D. Lhuillier, M. Cribier, and A. Letourneau. Reactor antineutrino anomaly. Phys. Rev. D, 83:073006, Apr 2011.
- [23] Ulrich Mosel. Neutrino event generators: foundation, status and future. J. Phys. G, 46(11):113001, 2019.
- [24] Lark Parsing Library & Toolkit. Lark. <https://github.com/lark-parser/lark>, 2017.